sustainability

MDPI

Article

What Drives Vegetation Evolution in the Middle Reaches of the Yellow River Basin, Climate Change or Human Activities?

Mengmeng Gao [1,2], Nan Yang [1,2,3,*] and Qiong Liu [1,2]

[1] China Institute of Geological Environmental Monitoring, Beijing 100081, China; gaomm_321@163.com (M.G.); shhhj05@163.com (Q.L.)
[2] Key Laboratory of Mining Ecological Effects and System Restoration, Ministry of Natural Resources, Beijing 100081, China
[3] Institute of Geophysical and Geochemical Exploration, Chinese Academy of Geological Sciences, Langfang 065000, China
* Correspondence: 13581631942@163.com

Abstract: The middle reaches of the Yellow River Basin (MYRB) are known for their significant soil erosion and fragile ecological environment, where vegetation growth is important. However, the vegetation's reaction to climate change (CC) and human activity (HA), and the potential driving mechanisms underlying such changes in the MYRB, have not yet been clarified. Thus, based on remote sensing data, combined with trend analysis and the Hurst method and supplemented by the structural equation model (SEM) and residual analysis method, we aimed to conduct an analysis of the spatio-temporal evolution of the normalized difference vegetation index (NDVI) in the MYRB from 2000 to 2020. Additionally, we explored how climate and human factors together affect the NDVI and quantified the proportion of their respective contributions to NDVI change. The NDVI exhibited a fluctuating upward trend in the MYRB. Moreover, approximately 97.7% of the area showed an improving trend, with nearly 50% of the area continuing to maintain an improving trend. Precipitation and temperature had positive effects on the NDVI, while vapor pressure deficit (VPD) and land use intensity (LUI) had negative effects. HA played a pivotal role in the vegetation improvement area with a contribution rate of 67.53%. The study revealed NDVI variations and emphasized the influence of HA on the NDVI in the MYRB. The findings are vital in comprehending the response mechanism of ecosystems and guiding reasonable environmental protection policies, which is beneficial for the sustainable development of the region.

Keywords: normalized difference vegetation index (NDVI); driving factors; residual analysis; structural equation model; middle reaches of the Yellow River Basin (MYRB)

Citation: Gao, M.; Yang, N.; Liu, Q. What Drives Vegetation Evolution in the Middle Reaches of the Yellow River Basin, Climate Change or Human Activities? *Sustainability* **2024**, *16*, 10122. https://doi.org/10.3390/su162210122

Academic Editors: Amos Darko, K. Venkatachalam, Baojie He, Ali Cheshmehzangi and Siliang Yang

Received: 29 September 2024
Revised: 14 November 2024
Accepted: 18 November 2024
Published: 20 November 2024

1. Introduction

As an essential component of ecosystems, vegetation is a key indicator of global terrestrial ecosystem changes and ecological environmental evolution [1–3] and thus is crucial for global water balance, surface energy exchange, and biogeochemical cycling [4,5]. With the impact of climate change (CC) and human activity (HA) in recent decades, the study of vegetation's enduring patterns, and its reactions to worldwide environmental shifts, has emerged as a prominent topic within ecological research endeavors [6].

The normalized difference vegetation index (NDVI), serving as a reliable metric for assessing the development of vegetation across regions, accurately identifies changes in plant cover and has gained extensive application in many key fields such as ecological monitoring, agricultural management, climate change research, and environmental protection [7–9]. Previous studies have reported that variations in vegetation exhibit a significant response to CC and revealed that the spatial heterogeneity of climatic conditions play decisive roles in vegetation change at the regional scale [10]. Temperature, precipitation, solar radiation,

relative humidity, carbon dioxide concentration, nitrogen deposition, and saturated vapor pressure differences are crucial climatic variables that significantly impact vegetation development and growth [11–14]. Globally, the repercussions of human activities on the NDVI have sparked extensive concerns, and varying patterns of change are exhibited across diverse regions. In Sub-Saharan Africa, for instance, rapid population growth fuels an escalating demand for agricultural land and forest products, thereby counteracting the climate-driven expansion of shrubland vegetation [15]. Conversely, deforestation driven by mining activities in the Amazon rainforest contributes to a decline in NDVI values [16]. In China, human activities such as urbanization, agricultural activities, the Grain for Green project, overgrazing, and tourism development have significantly contributed to changes in the NDVI [17–19].

CC and HA have a significant impact on vegetation growth. Although many scholars have used correlation analysis and multiple regression analysis in different regions to explore the influencing factors of the NDVI [20,21], the research on its driving mechanism is not yet sufficiently in-depth. This is because ordinary linear correlation analysis and multiple regression analysis do not consider the interrelationships between multiple independent variables, as well as the direct and indirect effects of independent variables on the dependent variable. Therefore, we introduced structural equation modeling (SEM), which can handle complex relationships between multiple variables, clarify driving paths, and provide a deeper understanding and recognition of driving mechanisms.

In previous studies, many scholars have adopted various exploration approaches to distinguish the impact of CC and HA on vegetation. Zhang [22] used a partial derivative method to decompose the interannual variation of vegetation change into the contributions of CC and HA in the Three River Headwaters Region, but did not specify the contribution rates of the CC and HA. Huang [23] introduced a GA–SVM model to quantify the effects of CC and HA on vegetation. This method combines the advantages of genetic algorithms and support vector machines, but its results are highly dependent on parameter selection, and different parameter combinations may lead to significant differences in results, which brings a lot of uncertainty to the results. The residual analysis method was used in this study to distinguish the impacts of CC and HA, which has been widely applied in previous studies [24,25]. The residual analysis method can reflect the comprehensive impact of CC and HA on vegetation change based on the difference between model predicted values and actual observed values, and can present the spatial distribution differences of contribution rates.

Previous research has highlighted pronounced geospatial disparities in the reaction of vegetation to CC and HA, suggesting that a complex and varied interplay between these factors influences the NDVI. Thus, specific analyses must be performed for different regions [26]. However, the response patterns of vegetation in the middle reaches of the Yellow River Basin (MYRB) to climate and human factors have not been clarified and must be investigated further.

Based on the MODIS NDVI dataset, meteorological data, and human activity data, this research explored the dynamic fluctuations in vegetation characteristics in the MYRB and quantitatively assessed the respective contributions of CC and HA to the variations in NDVI. The research objectives were to (1) analyze spatiotemporal dynamic changes of vegetation in the MYRB from 2000 to 2020; (2) analyze the key driving factors and the interplay between vegetation variations and key influencing factors; and (3) determine the respective contribution rates of CC and HA to NDVI change. This study can provide a scientific basis for the sustainable development of regional ecological environments.

2. Materials and Methods

2.1. Study Area

The MYRB is located in northern central China (Figure 1) and corresponds to the Yellow River Basin from Hekou Town in the Inner Mongolia Autonomous Region to Sanmenxia in Henan Province. Thus, it spans the six provinces of Ningxia, Gansu, Shaanxi, Shanxi, Inner

Mongolia, and Henan and covers a total area of 345,000 km^2. The terrain is high in the west and low in the east, with an average elevation of 85–3929 m (Figure 1a). The primary types of land encompass grassland, cropland, and forest land (Figure 1b). The region features a continental monsoon climate, exhibiting a gradient of declining precipitation and temperature from the southeast towards the northwest. Moreover, 61% of the watershed area is in the Loess Plateau [27], which has sparse vegetation, serious soil erosion, and an extremely fragile ecological environment. The MYRB is divided into three subwatersheds: Hekou to Longmen (HL); Longmen to Sanmenxia (LS); and Sanmenxia to Huayuankou (SH), accounting for 32.9%, 55.27%, and 11.83% of the total area, respectively (Figure 1c). The MRYB is a typical fragile ecological environment in China, and the regional vegetation development is the result of both natural factors and anthropogenic influences.

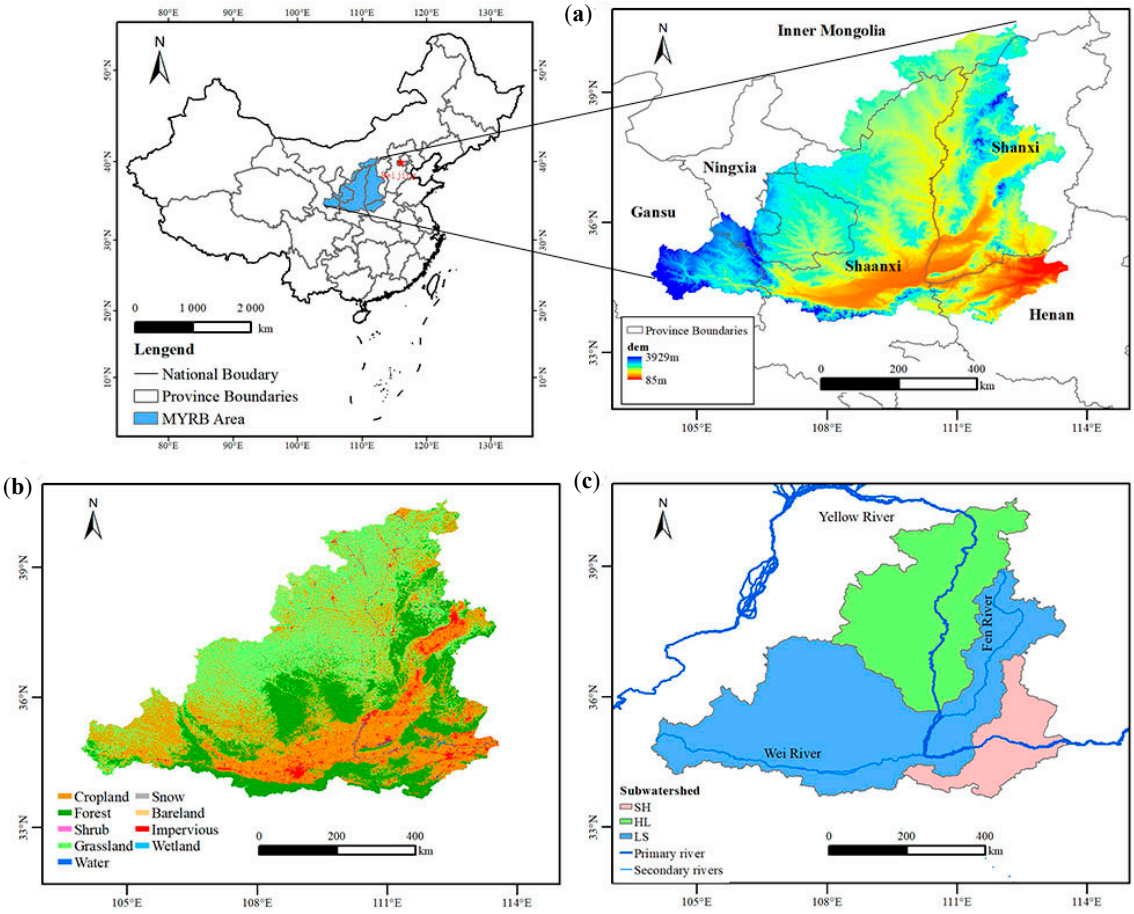

Figure 1. (**a**) Geographical location and topography; (**b**) land use in 2020; (**c**) subwatersheds of the middle reaches of the Yellow River Basin (MYRB).

2.2. Data Sources and Processing

2.2.1. MODIS Data

The NDVI is currently the most common indicator of vegetation growth. Higher NDVI values suggest better vegetation growth, whereas lower NDVI values suggest worse vegetation growth [28,29]. The NDVI data used were derived from the MOD13Q1 product, which was accessed via the NASA website, featuring a spatial resolution of 250 m and temporal resolution of 16 days (Table 1).

Table 1. Dataset information.

Data Name	Data Sources	Time Resolution	Spatial Resolution	Time Span	Data Type
NDVI	MOD13Q1	16 days	250 m	2000–2020	Grid
Precipitation	ERA5-land dataset	yearly	0.1°	2000–2020	Grid
Temperature	ERA5-land dataset	yearly	0.1°	2000–2020	Grid
Solar radiation	ERA5-land dataset	yearly	0.1°	2000–2020	Grid
Saturated vapor pressure	ERA5-land dataset	monthly	0.1°	2000–2020	Grid
Actual water vapor pressure	ERA5-land dataset	monthly	0.1°	2000–2020	Grid
Relative humidity	ERA5-land dataset	monthly	0.1°	2000–2020	Grid
Land use data	China Land Cover Dataset (CLCD)	yearly	30 m	2000–2020	Grid
Population density	Worldpop center	yearly	1 km	2000–2020	Grid

2.2.2. Climatological Data

The climatological data used in this study were derived from the ERA5-land dataset (https://cds.climate.copernicus.eu/, accessed on 28 September 2023), from which precipitation, temperature, and solar radiation (RAD) data can be obtained. Vapor pressure deficit (VPD) data cannot be obtained directly and must be obtained by calculation; the calculation formulas are available in referenced studies [30,31]. The data used in the calculations were also derived from the ERA5-land dataset. The spatial resolution of these data was 0.1° × 0.1°, and the resolution after resampling was 250 m, which was consistent with the NDVI data.

2.2.3. Land Use Data

Land use data featuring a 30 m resolution were acquired from the annual China Land Cover Dataset [32]. Land cover was classified into nine types: cropland (CL); forest (FL); shrubland (SL); grassland (GL); water land (WL); snow/ice (S/I); bareland (BL); impervious land (IL); and wetland (WL).

Land use intensity (LUI) represents the degree of human intervention in land use. Different land use categories are assigned values according to the degree of human intervention [33,34]; the calculation formula is as follows:

$$\mathrm{LUI} = \sum_{i=1}^{n} (A_i / A) \times 100 \times C_i \quad (1)$$

where A is the total area (km^2), n is the count of land use categories, A_i is the area of each land use categories (km^2), and C_i is the value of land use intensity for the i-th category of land use.

2.2.4. Population Data

Population density data, originally at a 1 km resolution, were sourced from the Worldpop Center (https://hub.worldpop.org/, accessed on 28 September 2023). These data were then resampled to align with a 250 m resolution, ensuring consistency with the NDVI data.

2.3. Methods

2.3.1. Trend Analysis and Significance Testing

The Theil–Sen median method was used to study the rate of change, which was calculated as follows:

$$slope = Median\left(\frac{\mathrm{NDVI}_j - \mathrm{NDVI}_i}{j - i}\right), \forall j > i \quad (2)$$

where *slope* is the variation trend, NDVI_i and NDVI_j are the NDVI values in years i and j, respectively, and i is the count of serial years.

The Mann–Kendall significance test [22] is expressed as follows:

$$S = \sum_{j=1}^{n-1} \sum_{i=j+1}^{n} sgn(\mathrm{NDVI}_i - \mathrm{NDVI}_j) \quad (3)$$

where n is the count of years, NDVI_i and NDVI_j are the NDVI values in years i and j ($j > i$), respectively, and $sgn(\mathrm{NDVI}_i - \mathrm{NDVI}_j)$ can be determined using Equation (4):

$$sgn(\mathrm{NDVI}_i - \mathrm{NDVI}_j) = \begin{cases} 1, \mathrm{NDVI}_i - \mathrm{NDVI}_j > 0 \\ 0, \mathrm{NDVI}_i - \mathrm{NDVI}_j = 0 \\ -1, \mathrm{NDVI}_i - \mathrm{NDVI}_j < 0 \end{cases} \quad (4)$$

When $n > 10$, the standard normal distribution variable was calculated using the following formula:

$$Z = \begin{cases} \frac{S-1}{\sqrt{Var(S)}}, S > 0 \\ 0, \quad S = 0 \\ \frac{S+1}{\sqrt{Var(S)}}, S < 0 \end{cases} \quad (5)$$

$$\sqrt{Var(S)} = n(n-1)(2n+5)/18 \quad (6)$$

where Z is a significant statistical variable and $Var(S)$ is the variance function. For a given confidence level α, if $|Z| \geq Z\_(1\text{-}\alpha/2)$, then a significant upward or downward trend occurred in the time series data. When $|Z|$ is greater than 1.96 and 2.58, it indicates that the trend has passed the significance test with confidence levels of 0.05 and 0.01, respectively. The Mann–Kendall test trend categories are shown in Table 2.

Table 2. Mann–Kendall test trend categories.

Trend Features	*Slope*	$\|Z\|$
Extremely significant decrease	*Slope* < 0	$\|Z\| > 2.58$
Significant decrease	*Slope* < 0	$1.96 < \|Z\| \leq 2.58$
No significant changes	—	$\|Z\| \leq 1.96$
Significant increase	*Slope* > 0	$1.96 < \|Z\| \leq 2.58$
Extremely significant increase	*Slope* > 0	$\|Z\| > 2.58$

2.3.2. Hurst Exponent Analysis

The Hurst exponent, first introduced by Hurst [35] and further refined by Mandelbrot and Wallis [36], was employed as a tool to forecast the future trends of NDVI changes [37,38]. This formula has been previously presented in [39,40].

H is the Hurst exponent, which ranges from 0 to 1 and is classified into three grades. When H = 0.5, randomness occurred in the data. When H > 0.5, the future trend is consistent with that of the past. When H < 0.5, the future trend is inconsistent with that of the past.

2.3.3. Residual Analysis

Residual analyses were performed to quantitatively describe the influences of CC and HA on NDVI changes. To derive the predicted NDVI values under the influence of climatic variation, a multiple regression model linking observed NDVI values with diverse parameters was formulated at the pixel scale. The divergence between the observed and predicted values was considered as the NDVI under the human-induced effects.

$$NDVI_{pre} = a \times P + b \times T + c \times R + d \times V + e \quad (7)$$

$$NDVI_{res} = NDVI_{obs} - NDVI_{pre} \quad (8)$$

where a, b, c, d, and e are regression coefficients, and P, T, R, and V are the precipitation, temperature, solar radiation, and vapor pressure difference, respectively. $NDVI_{res}$, $NDVI_{obs}$, and $NDVI_{pre}$ are the residual, observed, and predicted NDVI values, respectively.

The standards for identifying the factors driving changes in the NDVI (Appendix A) were defined based on previous studies [41].

2.3.4. Structural Equation Modeling

Structural equation modeling (SEM), a type of multivariate statistical analysis, is grounded in the examination of covariance matrices [42]. It can simultaneously handle the relationship between multiple dependent and independent variables, thus gaining deeper insights into the underlying processes and factors that could cause fluctuations in NDVI values.

3. Results

3.1. The Annual Average NDVI

The MYRB region exhibited a range of multiyear average NDVI values spanning from 0 to 0.79 (areal average value of 0.39), demonstrating a diverse vegetation cover over the years, and obvious spatial heterogeneity (Figure 2). The overall geographical arrangement was characterized by a "high in the southeast and low in the northwest" trend. The high NDVI values were mainly concentrated in the mountainous and hilly landscapes, including the elevated areas of the Liupanshan Mountains, the hilly areas of the Loess Plateau in the central area, the Luliang Mountains area, the mountainous area in southeastern Shanxi, and the Qinling Mountains area in the south, while the areas with low NDVI values were predominantly found in the hilly regions of the Loess Plateau, the Mu Us Sandy Land area, and the hilly areas of the Loess Plateau and Yellow Loess Ridges in the northwestern area. Combined with the land use categories, excluding impervious land, water, and snow/ice, the NDVI values from largest to smallest were ordered as follows: FL (0.61) > SL (0.57) > CL (0.44) > GL (0.37) > BL (0.18).

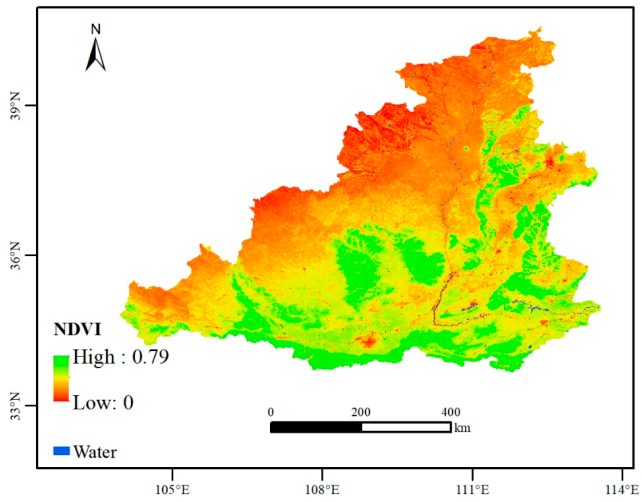

Figure 2. The annual average NDVI from 2000 to 2020 in the MYRB.

The annual average NDVI distribution differed notably among the different subwatersheds (Figure 3). HL showed a significant unimodal pattern, while SH showed a significant bimodal pattern, indicating that the type of land use and vegetation in the HL were relatively singular. The main land use type in HL was grassland, accounting for 67.99% of

the total area. However, there were two main vegetation types in SH, cropland and forest, accounting for 40.82% and 44.58%, respectively. Therefore, SH presented a bimodal pattern. The NDVI value corresponding to the part with the highest degree of density in SH was the largest and HL was the smallest, indicating that the vegetation growth of the SH was better than that of other subwatersheds. The interquartile range (IQR) in HL was the smallest at 0.09, indicating a more concentrated NDVI distribution, whereas the IQR in LS was the largest at 0.16, indicating a more discrete NDVI distribution. The maximum and minimum median NDVI values were recorded in SH (0.49) and HL (0.28), respectively. The NDVI values of the different subwatersheds, from highest to lowest, were ordered as follows: SH > LS > HL.

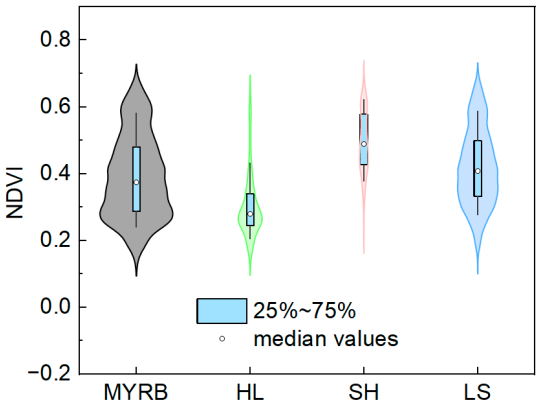

Figure 3. Violin plots of the annual average NDVI distribution in the different subwatersheds.

3.2. Temporal NDVI Changes

The NDVI in the MYRB showed an overall upward fluctuation trend, with an annual growth rate of 0.0063 (Figure 4). The NDVI value was the lowest in 2000 (0.31) and highest in 2018 (0.48). Moreover, the NDVI values of HL, LS, and SH showed an overall upward fluctuating trend and reached a peak in 2018. HL showed a significant trough in 2015, with NDVI values decreasing by 7.62% compared to that in the previous year. SH showed a significant trough in 2013, with NDVI values decreasing by 6.84% compared to those in the previous year, whereas the LS did not have a significant trough. Overall, the increasing tendency of the NDVI in HL was the largest, with an annual growth rate of 0.0074, whereas that in SH was the smallest, with an annual growth rate of 0.0052.

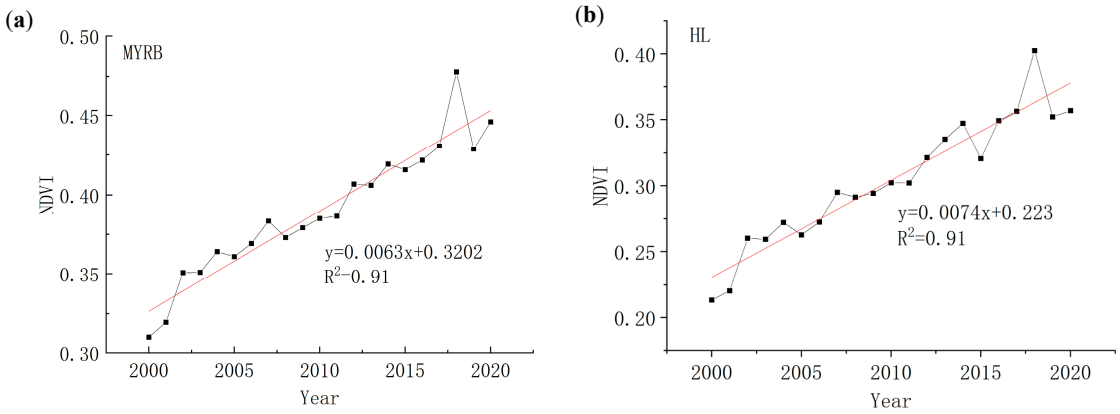

Figure 4. *Cont.*

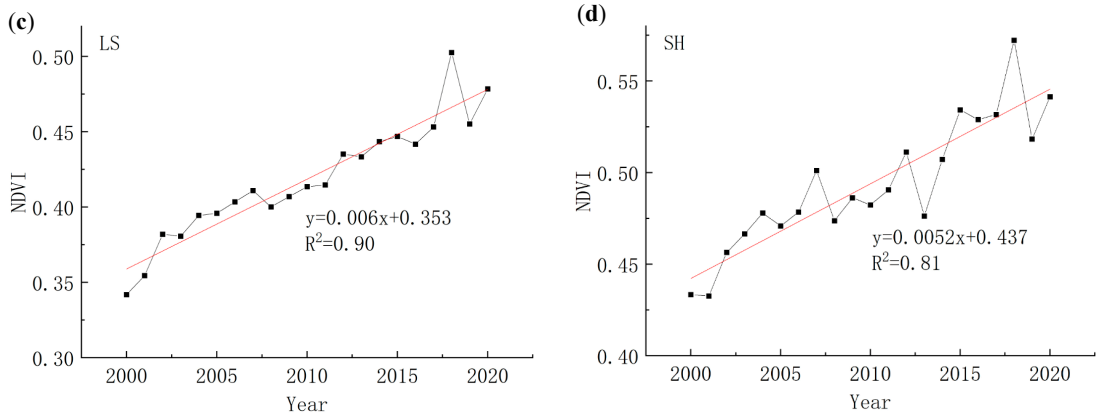

Figure 4. Inter-annual NDVI trends in (**a**) MYRB and its subwatersheds, (**b**) HL, (**c**) LS, (**d**) SH from 2000 to 2020.

3.3. Spatial Distributions of NDVI Variation Trend

The change rate of the NDVI spanned between −0.0026 and 0.0028 yr^{-1}, averaging at 0.0063 yr^{-1}. In terms of spatial variation, vegetation witnessed a positive trend in vegetation improvement in 97.7% of the total area of the MYRB from 2000 to 2020. Moreover, 94.41% of these regions demonstrated statistically significant improvement, primarily concentrated in the loess ridges, loess hills, and Mu Us Desert regions. The degraded area only accounted for 2.30%, of which 0.89% displayed statistical significance; this area was predominantly located in the Jinzhong and Guanzhong Basins (Figure 5).

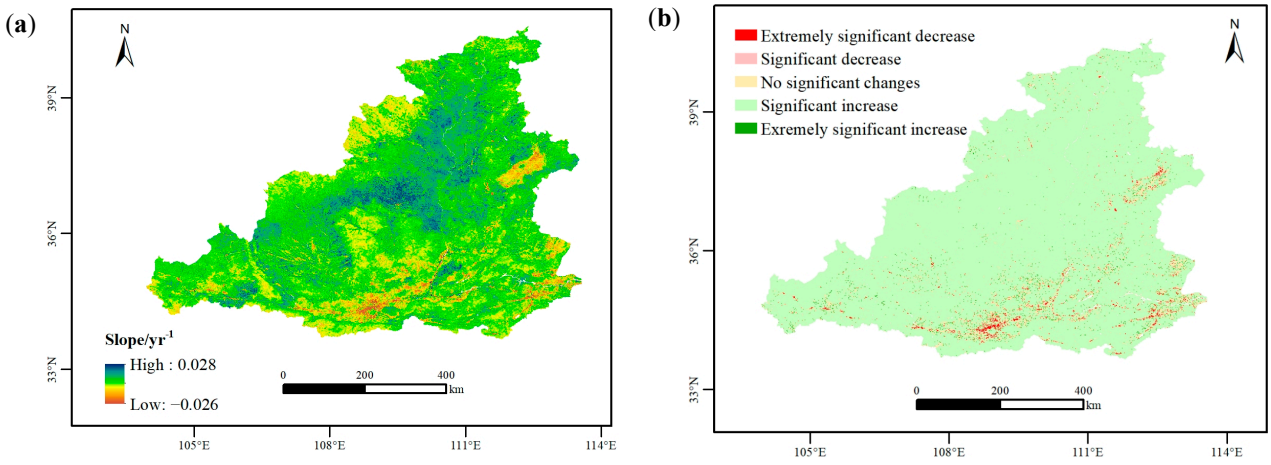

Figure 5. (**a**) Spatial distributions of slope of NDVI and (**b**) significant change in the MYRB.

From the perspective of the area of different NDVI trends in different watersheds, LS had the largest area of significant improvement in vegetation (including extremely significant and significant), about 177,329 km^2, while SH had the smallest area of significant improvement, about 36,515 km^2, and HL had a significant improvement area of about 111,999 km^2 (Figure 6a). From the perspective of the proportion of different NDVI trends in different watersheds, HL had the largest proportion of significantly improved vegetation areas (including extremely significant improvement and significant improvement) accounting for 98.61%, followed by LS and SH, accounting for 92.96% and 89.46%, respectively (Figure 6b).

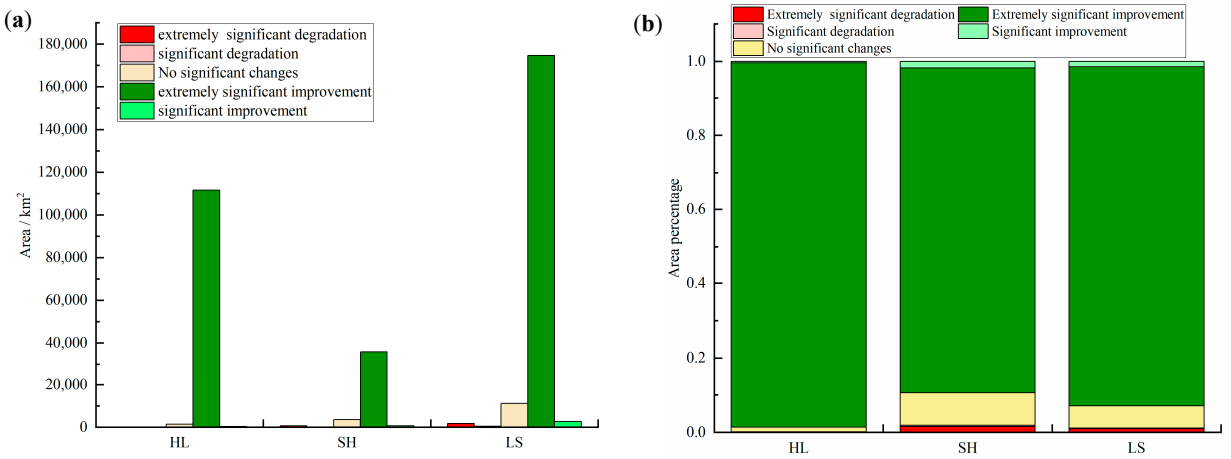

Figure 6. Area (**a**) and proportions (**b**) of different NDVI variation trends in different subwatersheds from 2000 to 2020.

Employing the Hurst exponent, we analyzed the future NDVI fluctuation patterns. The results indicated that the H values varied between 0.092 and 0.999, with an average of 0.503 (Figure 7a). The percentage of areas with H values exceeding 0.5 was 49.94%, suggesting that the current variation trend was sustainable, whereas the proportion of areas with H values less than 0.5 was 50.06%, indicating that the change trend was unsustainable (Figure 7b).

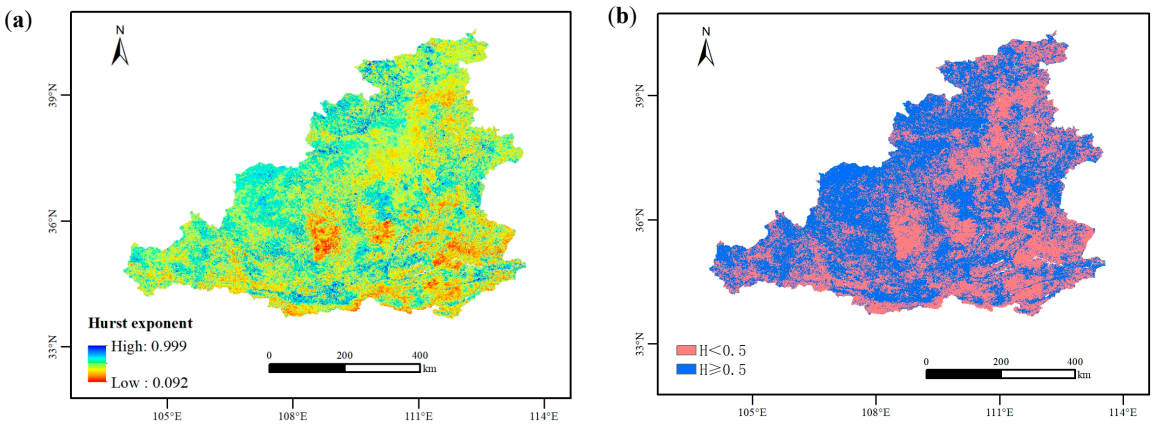

Figure 7. The (**a**) value and (**b**) classification of Hurst exponent of the NDVI in the MYRB.

By combining the Hurst exponent with the NDVI trends, a spatial distribution map of trend sustainability was obtained (Figure 8). The areas of consistently significant improvement accounted for 46.11% of the whole area, which accounted for 48.85% of all significantly improved areas, indicating that nearly half of the significantly improved area will continue this trend. The area of consistent significant degradation accounted for 0.70% of the whole area, which accounted for 79.65% of all significantly degraded area (Table 3). Combined with the land use categories, the predominant land use categories within the area that demonstrated consistently significant improvement were GL, CL, and FL, accounting for 39.15%, 26.47%, and 12.20%, respectively. These areas were distributed in the Mu Us Sandy land, loess hilly ridge, Fenwei Basin, and alpine hilly areas (Figure 9a). Among the areas of consistent significant degradation, the main land types were CL and CL converted into IL, accounting for 38.22% and 33.38%, respectively. These areas were predominantly situated around the Fenwei Basin and urban agglomerations in the eastern alluvial plain, which were related to urban expansion (Figure 9b).

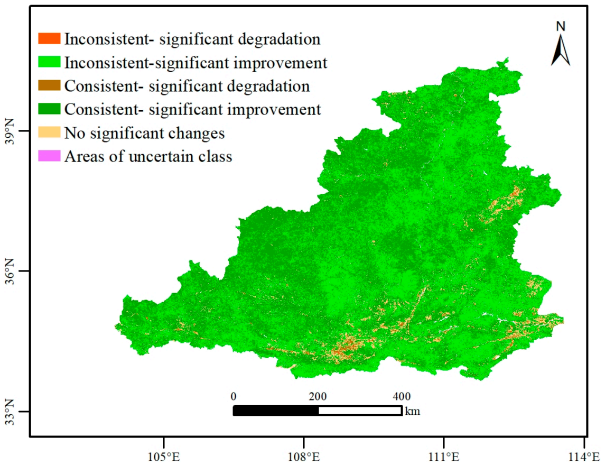

Figure 8. Trend sustainability in the MYRB.

Table 3. Proportion of area with trend sustainability in the MYRB.

Value	Sustainability	Area (%)
1	Inconsistent—significant degradation	0.19%
2	Inconsistent—significant improvement	48.29%
3	Consistent—significant degradation	0.70%
4	Consistent—significant improvement	46.11%
5	No significant changes	4.70%
6	Areas of uncertain class	0.00%
		100.00%

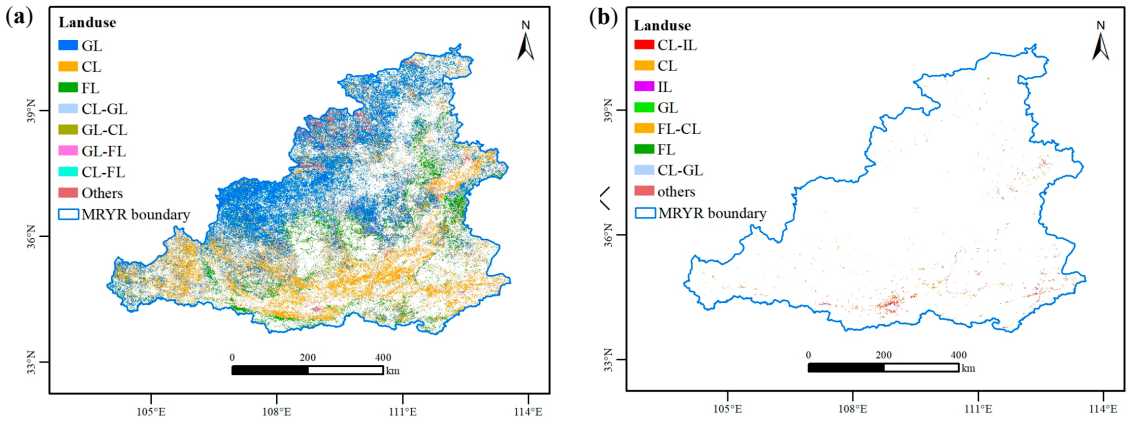

Figure 9. (**a**) Distribution map of land use conversion in the consistent significant improvement areas and (**b**) consistent significant degradation areas from 2000 to 2020. GL, grassland; CL, cropland; FL, forest land; IL, impervious land; and CL-GL, stands for cropland converted to grassland.

3.4. Comprehensive Analysis of Influencing Factors on NDVI

SEM was used to analyze how the driving factors affect NDVI trends. The factors affecting the NDVI included meteorological factors, which included hydrothermal conditions that affect vegetation growth, such as precipitation and VPD, representing hydrofactors; temperature and RAD, representing the thermal factors; and human activity factors, which included population density (PD) and LUI.

The results revealed that precipitation and temperature positively influenced the NDVI, exhibiting coefficients of 0.19 and 0.11, respectively, whereas VPD and LUI negatively influenced the NDVI, exhibiting coefficients of −0.08 and −0.17, respectively. PD and RAD had no significant impact on the NDVI (Figure 10).

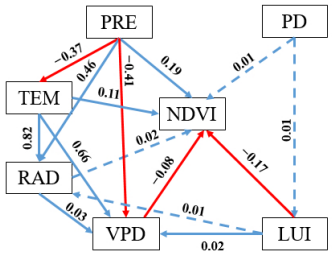

χ^2/df=1.523, CFI=1, p=0.166, RMSEA=0.006, n=16935

Figure 10. Structural equation modeling results for the NDVI dynamics driven by influencing factors. The solid blue single-arrow lines represent significant positive pathways ($p < 0.05$); The solid red single-arrow lines represent significant negative pathways ($p < 0.05$); Dashed arrows represent nonsignificant pathways ($p > 0.05$). Numbers placed next to the arrows represent the standardized path coefficients. PRE, precipitation; TEM, temperature; RAD, solar radiation; VPD, vapor pressure deficit; LUI, land use intensity; and PD, population density.

VPD represents air dryness, and precipitation has a negative impact on VPD, indicating that an increase in precipitation leads to a decrease in dryness and, consequently, an increase in the NDVI value. LUI, temperature, and RAD had positive impacts on VPD, indicating that the higher the LUI, RAD, and temperature, the drier the air and the higher the VPD.

3.5. Analysis of the Contributions of CC and HA to NDVI Changes

We used a residual analysis method to quantitatively evaluate the impact and relative contributions of CC and HA on vegetation growth changes.

The NDVI*pre* value reflects the impact of CC on the NDVI. The NDVI*pre* trend ranged between −0.026 and 0.025 yr^{-1}, averaging a rate of 0.002 yr^{-1} (Figure 11a). The proportion of the area in which CC contributed positively to the NDVI was 96.24%, and it was predominantly located in the loess hilly areas in the north and west and the mountainous hilly areas in the southeast. The proportion of the area in which CC contributed negatively to the NDVI was 3.76%, and it was predominantly located in the Guanzhong Basin and the Jinzhong Basin. The NDVI*res* values reflect the impact of HA on the NDVI. The NDVI*res* trend ranged between −0.019 and 0.019 yr^{-1}, averaging a rate of 0.004 yr^{-1} (Figure 11b). The proportion of the area in which HA contributed positively to the NDVI was 97.68%, and it was predominantly located in the loess ridge and hill areas in the northern and central regions and the high mountain areas in the western Liupan Mountains. The proportion of the area in which HA contributed negatively to the NDVI was 2.32%, and it was predominantly located in the urban agglomeration in the Fenwei Basin and the eastern alluvial plain.

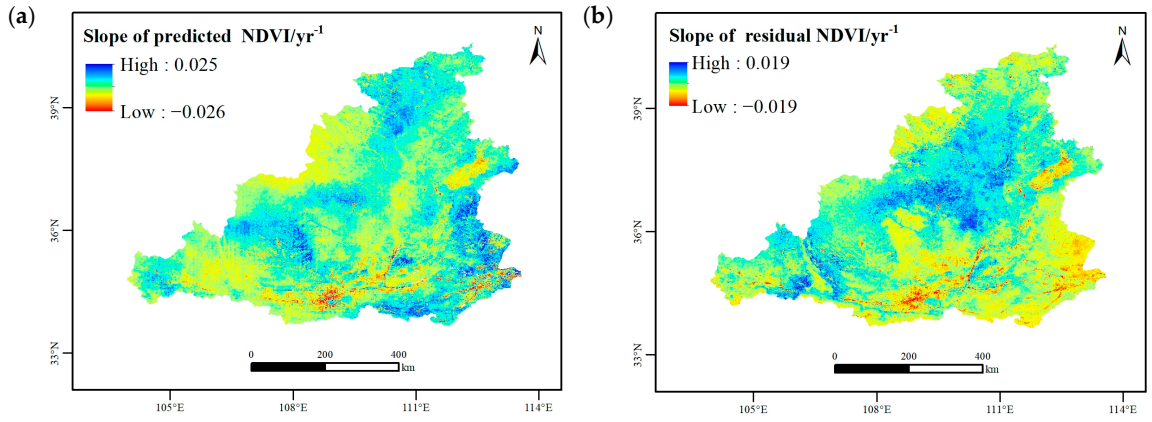

Figure 11. Trends of predicted (**a**) NDVI and (**b**) residual NDVI variations in the MRYB from 2000 to 2020.

The contribution percentages of both CC and HA towards the improvement and degradation of vegetation areas were calculated based on the predicted and residual values and the standard of driving factors. The results indicated that the vegetation improvement area affected by both CC and HA accounted for 97.7%, with CC contributing 32.47% and HA contributing 67.53% (Figure 12a,c). The area of vegetation degradation affected by both CC and HA accounted for 2.3%, with CC contributing 54.44% and HA contributing 45.56% (Figure 12b,d). HA dominated vegetation improvement, whereas CC dominated vegetation degradation.

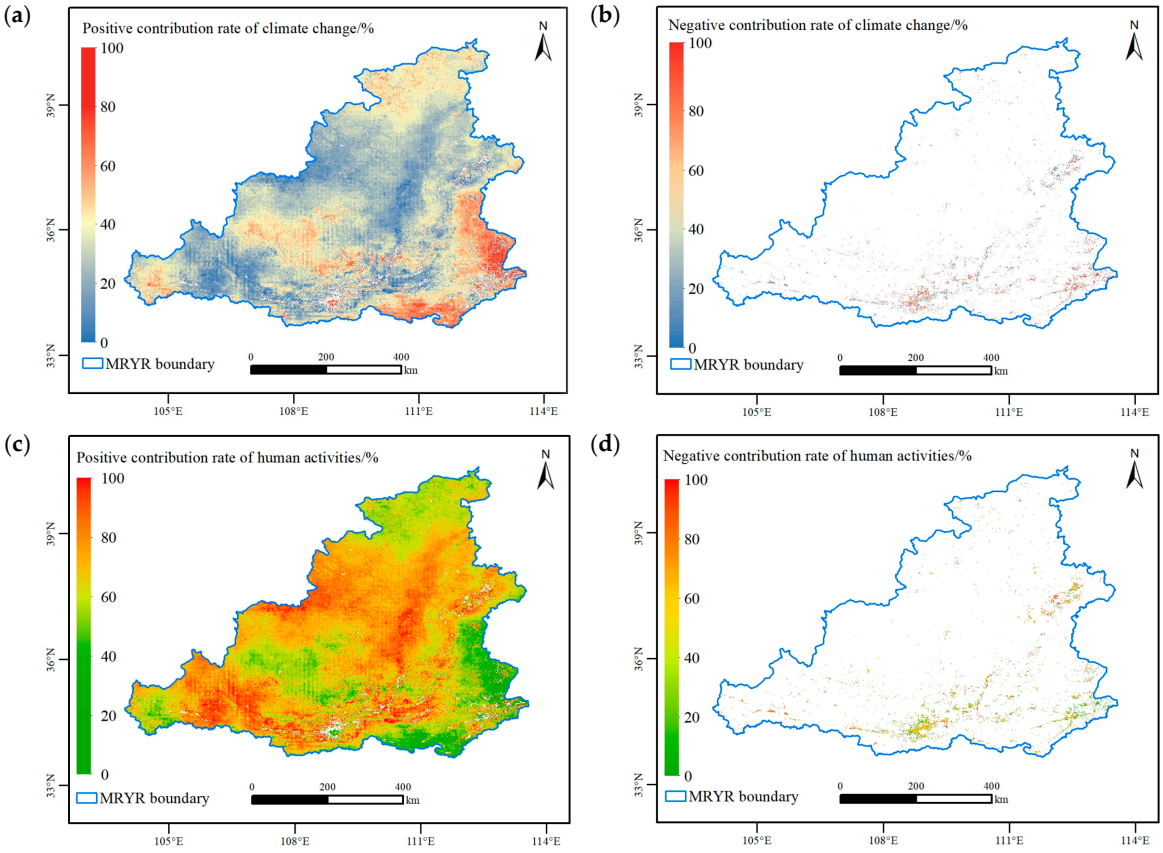

Figure 12. (**a**) Positive and (**b**) negative contributions of CC and (**c**) positive and (**d**) negative contributions of HA to NDVI in the MYRB from 2000 to 2020.

4. Discussion

4.1. NDVI Trend Analysis

We analyzed the evolving patterns of NDVI in the MYRB spanning the period from 2000 to 2020, and an upward trend was revealed. This result aligns with previous research on NDVI trends in China and the Yellow River Basin [43–46]. The areas with the most significant upward trend in NDVI were the Mu Us Sandy Land, Loess Plateau, and hilly areas. This upward trend is attributed to ecological projects during the last two decades. In 1999, the Chinese government embarked on a comprehensive series of ecological projects aimed at enhancing the environment [47], including the Grain for Green Project, the Three-North Shelterbelt Program Project, and the Natural Forest Protection Project. As an ecologically fragile area in the Yellow River Basin, it represents a typical area in which the aforementioned ecological projects have been implemented [48,49]. The implementation of ecological engineering has yielded remarkable outcomes in safeguarding farmland, conserving soil and water resources, mitigating wind erosion, and stabilizing sand dunes, and the regional ecological environment in the MYRB has been improved [50,51]. From 2000 to 2020, the CL area decreased, while the GL and FL areas increased. A total of 31,296.71 km^2 of CL has been transferred out, of which 3441.62 km^2 and 22,320.72 km^2

have been converted into FL and GL, respectively, accounting for 11% and 71.32% of the total transferred land area. This finding intuitively demonstrates the benefits of the Grain for Green project (Figure 13).

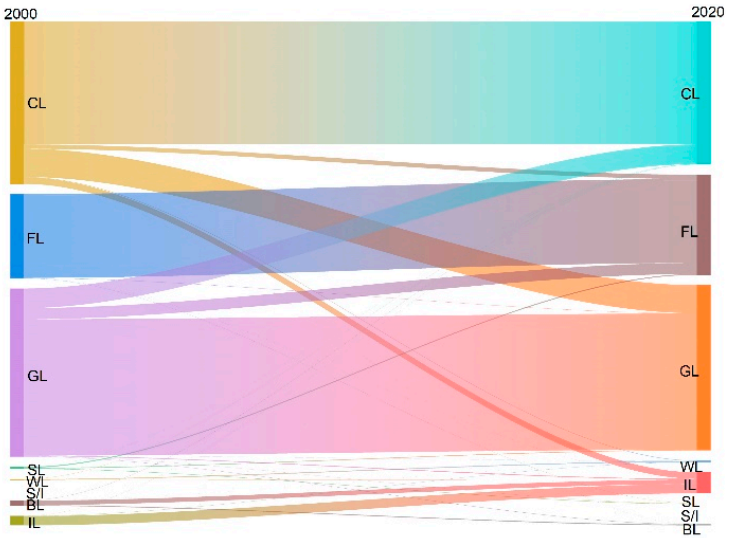

Figure 13. Sankey diagram of land use transfer. CL, cropland; FL, forest; SL, shrubland; GL, grassland; WL, water land; S/I, snow/ice; BL, bareland; IL, impervious land; and WL, wetland.

In terms of varying land use categories, the order of NDVI values from high to low was FL (0.61) > SL (0.57) > CL (0.44) > GL (0.37) > BL (0.18), which aligns with previous research findings [25]. However, the same types of land exhibited variations in NDVI values across different regions, which were intricately linked to external environmental conditions, including precipitation, temperature, terrain, and soil [52–54].

The annual average NDVI distribution differed notably among the different subwatersheds. The result showed that the NDVI value of SH was the largest, and that of HL was the smallest. HL had the highest percentage of areas with a significant improvement trend in vegetation. We analyzed the reasons for the variability of NDVI in the three subwatersheds in terms of climatic conditions and geomorphological types. HL flows through the Loess Plateau region, with loess hills and gullies as the main landforms. The Mu Us Sandy land is distributed in the area, and the main land use type is grassland. There is less precipitation, low vegetation coverage, and a fragile ecological environment. Therefore, SH exhibited the lowest NDVI. With the implementation of ecological engineering, grassland vegetation gradually recovered, and forest area increased, which is the reason why the area of the rising NDVI trend occupies the largest proportion in HL. The terrain of LS is undulating and complex, with loess landforms such as plateaus, ridges, and hills widely distributed. There are both high mountains and the Fenwei Basin distributed in the region, and the main land use types are cropland and grassland. The complexity of its landform type has resulted in its NDVI being at a moderate level. SH is a transitional section of the Yellow River from mountainous areas to plains, mainly presenting a valley plain landform with relatively high precipitation. Due to the widespread distribution of cropland and forest, the vegetation coverage is high, especially in mountainous and valley areas, where vegetation growth is lush. Therefore, LS exhibited a high NDVI.

4.2. Analysis of Factors That Influence NDVI Change

Previous research has extensively investigated the impact of various factors, notably meteorological factors, on changes in NDVI, as well as some factors such as climatic periods and seasonal changes [55–57]. A basic consensus has been reached that both precipitation and temperature have significant impacts on NDVI changes [58,59]. However, a consensus has not been reached on whether precipitation and temperature exert a positive

or negative influence on the NDVI, which is related to the geographical location, climate, and spatiotemporal scale [60,61].

Enhanced rainfall ensures the availability of water needed for vegetation growth by increasing soil moisture [62]. The promoting effect of precipitation on the NDVI is evident in arid and semi-arid areas, whereas excessive precipitation in humid areas can affect RAD, reduce vegetation photosynthesis, and negatively affect vegetation growth [63]. The MYRB belongs to arid and semi-arid areas, which supports the conclusion drawn in this study that precipitation positively influenced changes in the NDVI. Increasing temperatures facilitate the decomposition and liberation of soil organic matter and nutrients while simultaneously enhancing vegetation photosynthesis, which promotes vegetation growth [64]. Therefore, temperature positively influenced changes in the NDVI. VPD represents the dryness of the atmosphere, with a greater VPD indicating a drier atmosphere. When the VPD is high, plants adopt a protective mechanism by constricting their stomata to conserve water, which decreases photosynthesis and carbon uptake [65,66]. An increase in atmospheric VPD leads to a decrease in global vegetation growth [67]. Therefore, VPD negatively correlated with the NDVI.

LUI reflects the degree of human activity disturbance [68]. There are two types of land disturbances caused by human activities: the expansion of construction land caused by urbanization, occupation, and green space reduction, resulting in an increasing LUI and decreasing NDVI; and greenspace restoration under ecological restoration policies, resulting in a decreasing LUI and increasing NDVI. Therefore, LUI negatively correlated with the NDVI.

In order to more intuitively demonstrate the impact of LUI on NDVI, we analyzed the correlation between NDVI and LUI in temporal trend and spatial distribution. Moreover, we also analyzed the correlation between NDVI and LUI under different population density levels. In terms of temporal trends, LUI showed a downward trend from 2000 to 2020 (Figure 14a), while NDVI showed an upward trend (Figure 14b), with a negative correlation between NDVI and LUI (Figure 14c). The reason for the decline in LUI is mainly due to the significant increase in forest and grassland area, which is greater than the increase in impervious land area caused by urban expansion, indicating the significant effectiveness of ecological engineering implementation. In terms of spatial distribution, by taking NDVI as the gradient and dividing it into 30 levels, corresponding LUI values were extracted, and the correlation between the two was analyzed. The results showed that LUI and NDVI also exhibited a negative correlation in space (Figure 14d).

Furthermore, we divided population density into 20 levels using population density as a gradient, and then extracted the average values of LUI and NDVI on different population density gradients. We found that LUI and NDVI showed a reverse trend with increasing population density (Figure 15). The higher the population density, the higher the LUI and the lower the NDVI. This indicated that in areas where the population is concentrated, the intensity of land use is high, which will cause damage to the ecological environment.

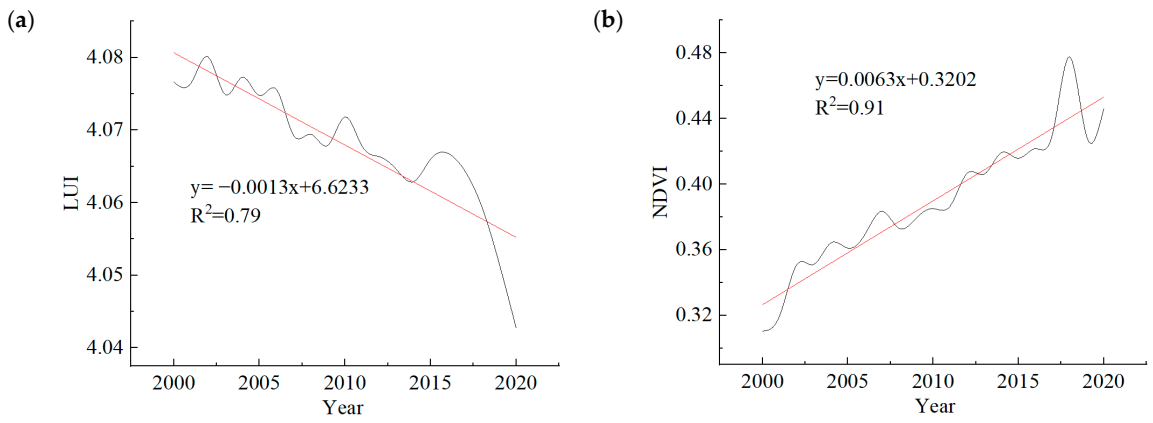

Figure 14. *Cont.*

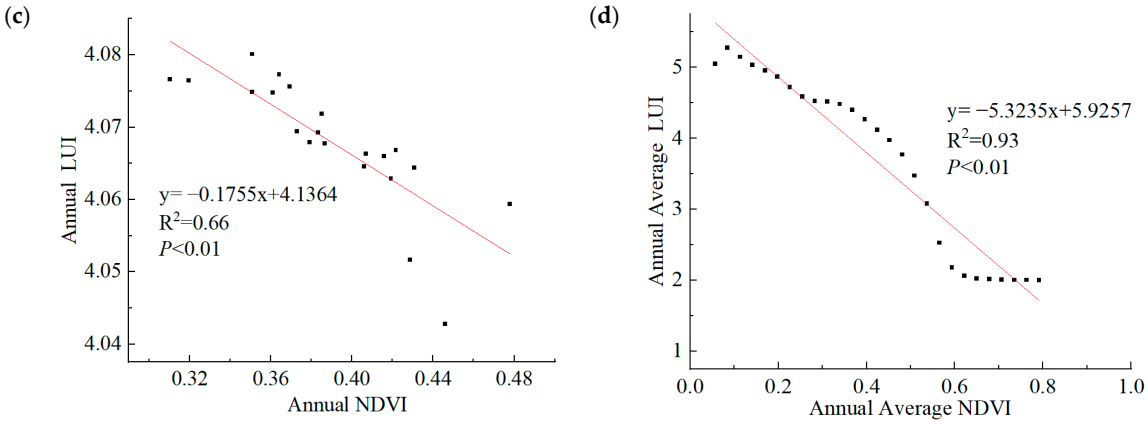

Figure 14. Change trend in (**a**) LUI and (**b**) NDVI; correlation of scatter plot between LUI and NDVI in terms of (**c**) temporal trends and (**d**) spatial distribution.

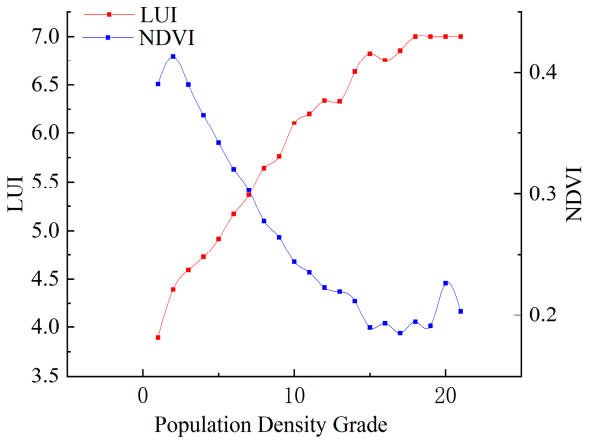

Figure 15. Change trend of LUI and NDVI in population density grade.

It can be seen that the population density level of 15 (approximately 20,000 people per square kilometer) was a crucial transition point. Below this density level, NDVI and LUI exhibited sharp trends of change and demonstrated a significant negative correlation. However, when the population density exceeded this level, the change in LUI and NDVI tended to flatten out. This suggested that when population concentration reaches 20,000 people per square kilometer, the intensity of LUI attained a relatively saturated state, while NDVI remained at a relatively stable but low level.

Moreover, the comparison between population density and NDVI can offer valuable insights into urban communities. The areas with high population density and low NDVI might indicate regions under stress due to limited green spaces and potentially higher demands on infrastructure and resources. Conversely, the zones with a more balanced relationship between the two could signify a healthier living environment.

In this study, RAD exhibited a positive influence on changes in the NDVI; however, the effect was not significant. Although RAD is a crucial factor in vegetation growth, the effects of other influencing factors on the NDVI are even more notable in the region. Thus, the effect of RAD on the NDVI may become insignificant under the comprehensive influence of numerous influencing factors.

4.3. Contribution of CC and HA to the NDVI

More than 95% of the area was a vegetation improvement zone dominated by HA, with a contribution percentage of 67.53%, whereas the contribution percentage of CC was only 32.47%. Approximately 2.3% of the area is a vegetation degradation zone, with HA and CC contributing roughly equal amounts at 45.56% and 54.44%, respectively. The findings

indicate that human interventions exert a more central and crucial influence than climatic factors in regulating annual NDVI changes in this region, as supported by previous studies on NDVI changes in China [69], the Qinghai-Tibet Plateau [59], and the Loess Plateau [70].

It was worth noting that CC contributed more to degradation than HA in certain areas (54.44% vs. 45.56%). Therefore, focusing on vegetation degradation areas, further analysis was conducted on the impact of meteorological factors on vegetation degradation. We extracted areas with a climate change contribution rate greater than 50% in vegetation degradation zones and analyzed the reasons for degradation in terms of climate change. The precipitation in this area showed a decreasing trend, while the VPD showed an increasing trend from 2000 to 2020 (Figure 16). Under a background of decreasing precipitation and increasing VPD, the decrease in NDVI reflected the negative impacts of drought stress and climate change on vegetation. The decrease in precipitation will directly affect the water supply of vegetation, resulting in vegetation growth restriction. The rise in VPD means that the water vapor content in the atmosphere is relatively low and the air is drier. Such dry climatic conditions will intensify water evaporation from vegetation, making vegetation more vulnerable to drought [67]. Meanwhile, the increase in VPD may also affect the photosynthesis of vegetation, further limiting its growth. Therefore, vegetation in this area showed a degraded state. We should focus on areas where precipitation will continue to decrease and VPD will continue to increase in the future.

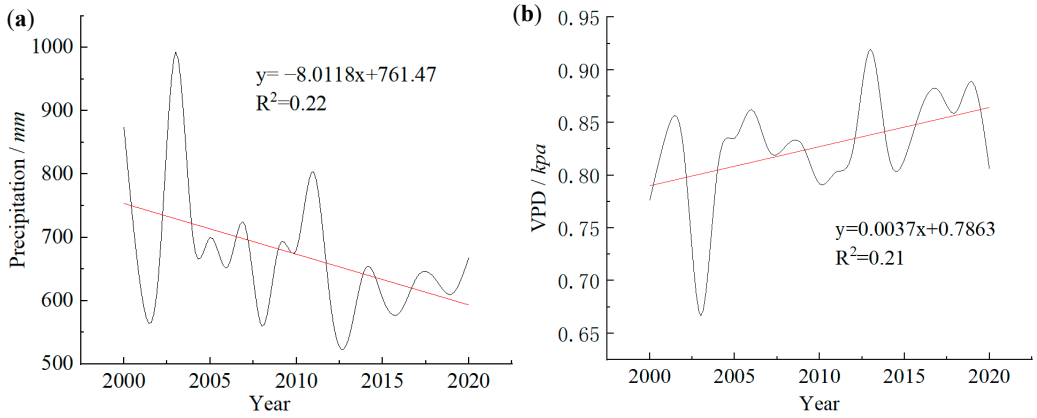

Figure 16. Change trend of (**a**) precipitation and (**b**) VPD in vegetation degradation areas.

4.4. Limitations and Uncertainties

MODIS NDVI, which is widely used in research on dynamic NDVI change trends worldwide, was used in this study. However, different sensors, such as MODIS and AVHRR, have different spectral characteristics and spatial resolutions, leading to differences in the calculation results. Therefore, combining multi-source data and further analyzing the uncertainties brought about by these different data sources is necessary to arrive at more reliable conclusions. In addition, although remote sensing data are convenient and easy to obtain, they cannot replace field observation data, which makes it difficult to evaluate the accuracy of NDVI. Therefore, further verification of the data accuracy is required to obtain more reliable results.

Although the ERA5-land dataset is a widely used climate data source, there are still uncertainties. For some rapidly changing climate events or small-scale climate heterogeneity regions, there is a problem of insufficient capture, such as short-term extreme climate events being smoothed out in the time-averaging process, thereby underestimating their impact on vegetation. Additionally, a resolution of 1 km is insufficient to accurately reflect the impact of climate conditions on vegetation in a small area.

In addition, climatic factors such as temperature, precipitation, RAD, and VPD were selected according to the hydrothermal conditions to investigate the influence of CC on the NDVI. However, these climatic factors cannot fully represent CC, with environmental factors, such as CO_2 concentration change and nitrogen deposition, also affecting vege-

tation [71]. Moreover, LUI cannot represent all human activities. Industrial emissions of pollutants such as sulfur dioxide, nitrogen oxides, and particulate matter may affect the photosynthesis and respiration of vegetation. High concentrations of atmospheric pollutants can deposit on the surface of leaves, hindering gas exchange in stomata and reducing photosynthetic efficiency, thereby affecting vegetation growth and NDVI values [72]. In addition, this study focused on the macro-scale watershed areas, but more factors need to be considered for the micro-scale of densely populated cities. For example, greening roofs of buildings, creating park areas and ecological corridors, as part of urban human activities, can alter the urban microclimate and have a dual impact on NDVI changes [73,74]. Therefore, the abovementioned environmental and human factors should be considered in further explorations of the response of vegetation change to CC and HA.

5. Conclusions

This study was conducted to explore the changes in vegetation cover (using NDVI as an indicator) and the driving mechanism during 2000–2020, and to determine the contributions of CC and HA in the MYRB. Remote sensing data analysis, trend analysis, Hurst index prediction, the SEM method, and the residual analysis method were employed in the analysis. The main findings are as follows:

(1) The NDVI in the MYRB showed a fluctuating upward trend, displaying an annual growth rate of 0.0063, indicating that vegetation coverage had improved. The overall geographical arrangement was characterized by a "high in the southeast and low in the northwest" trend.

(2) The vast majority (97.7%) of areas exhibited a pattern of vegetation enhancement, and 48.85% of the areas were expected to continue to maintain this trend of improvement. The improvement area was mainly concentrated in GL, FL, and CL.

(3) Through using the SEM method, precipitation, air temperature, VPD, and LUI were identified as the key driving factors affecting NDVI change. Precipitation and temperature exhibited a positive impact on vegetation, while VPD and LUI exhibited a negative effect.

(4) In the area of vegetation improvement, the contribution of HA was notably higher at 67.53%, significantly surpassing the influence of CC, which accounted for 32.47%. However, in the area of vegetation degradation, the contribution of CC (54.44%) was relatively higher. This indicates that, in the MYRB, the positive influence of HA on vegetation cover is significant; however, in some local areas or under certain conditions, CC may also be the dominant factor of vegetation degradation.

(5) In addition to urban expansion factors, the drought stress caused by reduced precipitation and increased VPD also limits vegetation growth in areas with vegetation degradation. The vegetation improvement area is mainly attributed to the implementation of ecological engineering. We suggest establishing a long-term monitoring and evaluation mechanism, regularly collecting and analyzing ecological indicator data, to promptly identify and solve problems, and provide scientific basis and decision-making support for future ecological restoration projects.

In summary, this study not only revealed the dynamic change characteristics of the NDVI in the MYRB; the relative contributions of CC and HA to vegetation change were also quantified, laying a scientific groundwork for local ecological conservation and sustainable growth. Future studies can further refine the characteristics of vegetation dynamics and its drivers under different land use categories, as well as explore more effective ecological protection and restoration strategies.

Author Contributions: Conceptualization, N.Y.; data curation, formal analysis and methodology, M.G.; supervision and validation, Q.L.; visualization, M.G. and Q.L.; writing—original draft, M.G.; writing—review and editing, Q.L. and N.Y. All authors have read and agreed to the published version of the manuscript.

Funding: This research is supported by the Geological Survey Project of National Water Resources Survey, Monitoring, Evaluation, and Smart Services (DD20230075) and Monitoring and Evaluation of

Resource and Environmental Carrying Capacity in National Major Regional Development Strategy Zones (DD20230117).

Institutional Review Board Statement: Not applicable.

Informed Consent Statement: Not applicable.

Data Availability Statement: The raw data supporting this paper can be obtained for free on relevant websites, and the website name or address was presented in the main text.

Acknowledgments: We thank Jin from the China University of Geosciences (Beijing) for providing the batch data processing program and tools, and we thank Liu from Beijing Forestry University for providing positive and constructive advice.

Conflicts of Interest: The authors declare no conflicts of interest.

Appendix A

The standards for identifying the driving factors of NDVI changes are shown in the following table.

Table A1. Standards for identifying the factors driving changes in the NDVI.

S(NDVI*obs*)	Driving Factor	Standards for the Classification		Contribution Rate/%	
		S(NDVI*pre*)	S(NDVI*res*)	CC	HA
>0	CC and HA	>0	>0	*S*(NDVI*pre*)/*S*(NDVI*obs*)	*S*(NDVI*res*)/*S*(NDVI*obs*)
Positive	CC	>0	<0	100	0
effects	HA	<0	>0	0	100
<0	CC and HA	<0	<0	*S*(NDVI*pre*)/*S*(NDVI*obs*)	*S*(NDVI*res*)/*S*(NDVI*obs*)
Negative	CC	<0	>0	100	0
effects	HA	>0	<0	0	100

S: slope of trend.

References

1. Foley, J.A.; Levis, S.; Costa, M.H.; Cramer, W.; Pollard, D. Incorporating dynamic vegetation cover within global climate models. *Ecol. Appl.* **2000**, *10*, 1620–1632. [CrossRef]
2. Jin, X.M.; Guo, R.H.; Zhang, Q.; Zhou, Y.X.; Zhang, D.R.; Yang, Z. Response of vegetation pattern to different landform and water-table depth in Hailiutu River basin, Northwestern China. *Environ. Earth Sci.* **2014**, *71*, 4889–4898.
3. Bohovic, R.; Dobrovolny, P.; Klein, D. The spatial and temporal dynamics of remotely-sensed vegetation phenology in central Asia in the 1982–2011 period. *Eur. J. Remote Sens.* **2016**, *49*, 279–299. [CrossRef]
4. Betts, R.A. Global vegetation and climate: Self-beneficial effects, climate forcings and climate feedbacks. *J. Phys. IV (Proc.)* **2004**, *121*, 37–60. [CrossRef]
5. Zhu, L.K.; Southworth, J. Disentangling the Relationships between Net Primary Production and Precipitation in Southern Africa Savannas Using Satellite Observations from 1982 to 2010. *Remote Sens.* **2013**, *5*, 3803–3825. [CrossRef]
6. Piao, S.L.; Yin, G.D.; Tan, J.G.; Cheng, L.; Huang, M.T.; Li, Y.; Liu, R.G.; Mao, J.F.; Myneni, R.B.; Peng, S.S.; et al. Detection and attribution of vegetation greening trend in China over the last 30 years. *Glob. Chang. Biol.* **2015**, *21*, 1601–1609. [CrossRef]
7. Wang, H.J.; Li, Z.; Cao, L.; Feng, R.; Pan, Y.P. Response of NDVI of natural vegetation to climate changes and drought in China. *Land* **2021**, *10*, 966. [CrossRef]
8. Francisco, C.; Elizabeth, A.S.; Simón, C.B.D.; David, M.C. A Forecast Model Applied to Monitor Crops Dynamics Using Vegetation Indices (NDVI). *Appl. Sci.* **2021**, *11*, 1859. [CrossRef]
9. Mehmood, K.; Anees, A.S.; Rehman, A.; Pan, S.A.; Tariq, A.; Zubair, M.; Liu, Q.J.; Rabbi, F.; Khan, K.A.; Luo, M. Exploring spatiotemporal dynamics of NDVI and climate-driven responses in ecosystems: Insights for sustainable management and climate resilience. *Ecol. Inform.* **2024**, *80*, 102532. [CrossRef]
10. Seddon, A.W.R.; Macias-Fauria, M.; Long, P.R.; Benz, D.; Willis, K.J. Sensitivity of global terrestrial ecosystems to climate variability. *Nature* **2016**, *531*, 229–232. [CrossRef]
11. Dai, A. Increasing drought under global warming in observations and models. *Nat. Clim. Chang.* **2013**, *3*, 52–58. [CrossRef]
12. Ding, Y.X.; Li, Z.; Peng, S.Z. Global analysis of time-lag and -accumulation effects of climate on vegetation growth. *Int. J. Appl. Earth Obs. Geoinf.* **2020**, *92*, 102179. [CrossRef]
13. Zhe, M.; Zhang, X.Q. Time-lag effects of NDVI responses to climate change in the Yamzhog Yumco Basin, South Tibet. *Ecol. Indic.* **2021**, *124*, 107431. [CrossRef]

14. Wang, X.; Zhao, F.; Wu, Y. Increased sensitivity of vegetation to soil moisture and its key mechanisms in the Loess Plateau, China. *Ecohydrology* **2023**, *17*, 6239. [CrossRef]
15. Martin, B.; Kjeld, R.; Josep, P.; Feng, T.; Guy, S.; Aleixandre, V.; Ole, M.; Rb, P.J.; Rasmus, F. Human population growth offsets climate-driven increase in woody vegetation in sub-Saharan Africa. *Nat. Ecol. Evol.* **2017**, *1*, 81.
16. Fábio, C.; Mello, F.A.O.; Mahboobeh, T.; Lucas, S.J.; Rabelo, C.L.; Accorsi, A.M.T.; Pimenta, B.S.G.; Osório, F.T.; Francisco, R.; Fabio, P.; et al. Impact of mining-induced deforestation on soil surface temperature and carbon stocks: A case study using remote sensing in the Amazon rainforest. *J. S. Am. Earth Sci.* **2022**, *119*, 103983.
17. Yi, L.; Sun, Y.; Ouyang, X.; Yin, S.H. Identifying the Impacts of Climate Change and Human Activities on Vegetation Cover Changes: A Case Study of the Yangtze River Basin, China. *Int. J. Environ. Res. Public. Health* **2022**, *19*, 6239. [PubMed]
18. Wang, J.; Meng, J.J.; Cai, Y.L. Assessing vegetation dynamics impacted by climate change in the southwestern karst region of China with AVHRR NDVI and AVHRR NPP time-series. *Environ. Geol.* **2007**, *54*, 1185–1195.
19. Sun, L.; Li, H.; Wang, J.; Chen, Y.H.; Xiong, N.N.; Wang, Z.; Wang, J.; Xu, J.Q. Impacts of Climate Change and Human Activities on NDVI in the Qinghai-Tibet Plateau. *Remote Sens.* **2023**, *15*, 587. [CrossRef]
20. Xue, X.; Wang, Z.; Hou, S.S. NDVI-Based Vegetation Dynamics and Response to Climate Changes and Human Activities in Guizhou Province, China. *Forests* **2023**, *14*, 753. [CrossRef]
21. Liu, Y.G.; Zhang, X.K.; Du, X.D.; Du, Z.Y.; Sun, M.Z. Alpine grassland greening on the Northern Tibetan Plateau driven by climate change and human activities considering extreme temperature and soil moisture. *Sci. Total Environ.* **2024**, *916*, 169995. [CrossRef]
22. Zhang, X.C.; Jin, X.M. Vegetation dynamics and responses to climate change and anthropogenic activities in the Three-River Headwaters Region, China. *Ecol. Indic.* **2021**, *131*, 108223. [CrossRef]
23. Huang, S.Z.; Zheng, X.D.; Ma, L.; Wang, H.; Huang, Q.; Leng, G.Y.; Meng, E.H.; Guo, Y. Quantitative contribution of climate change and human activities to vegetation cover variations based on GA-SVM model. *J. Hydrol.* **2020**, *584*, 124687. [CrossRef]
24. Liu, R.; Xiao, L.L.; Liu, Z.; Dai, J.C. Quantifying the relative impacts of climate and human activities on vegetation changes at the regional scale. *Ecol. Indic.* **2018**, *93*, 91–99. [CrossRef]
25. Ma, M.; Wang, Q.; Liu, R.; Zhao, Y.; Zhang, D. Effects of climate change and human activities on vegetation coverage change in northern China considering extreme climate and time-lag and accumulation effects. *Sci. Total Environ.* **2023**, *860*, 160527. [CrossRef]
26. Xu, L.; Myneni, R.B.; Chapin, F.S., III; Callaghan, T.V.; Pinzon, J.E.; Tucker, C.J.; Zhu, Z.; Bi, J.; Ciais, P.; Tømmervik, H.; et al. Temperature and vegetation seasonality diminishment over northern lands. *Nat. Clim. Chang.* **2013**, *3*, 581–586. [CrossRef]
27. Zhao, X.Y.; Du, Y.X.; Li, H.; Wang, W.J. Spatio-temporal changes of the coupling relationship between urbanization and ecosystem services in the Middle Yellow River. *J. Nat. Resour.* **2021**, *36*, 131–147. [CrossRef]
28. Jin, X.M.; Wan, L.; Zhang, Y.K.; Hu, G.C.; Schaepman, M.E.; Clevers, J.G.P.W.; Su, Z.B. Quantification of spatial distribution of vegetation in the Qilian Mountain area with MODIS NDVI. *Int. J. Remote Sens.* **2009**, *30*, 5751–5766. [CrossRef]
29. Gao, M.M.; Liu, Q.; Wang, Y.; Li, X.L.; Shi, P. Spatial and temporal variations in vegetation index and its impact factors in the West Liaohe Plain in Inner Mongolia. *Hydrogeol. Eng. Geol.* **2022**, *49*, 175–182. [CrossRef]
30. Gao, M.M.; Liu, Q.; Liu, Y.L.; Yang, N.; Wang, Y.; Li, X.L. Spatial and temporal variations of vegetation water use efficiency and its response to climate change and human activities in the West Liao River Plain, China. *Front. Ecol. Evol.* **2023**, *11*, 1176131. [CrossRef]
31. Li, Z.X.; Feng, Q.; Liu, W.; Wang, T.T.; Gao, Y.; Wang, Y.M.; Cheng, A.F.; Li, J.G.; Liu, L. Spatial and temporal trend of potential evapotranspiration and related driving forces in Southwestern China, during 1961–2009. *Quat. Int.* **2014**, *336*, 127–144.
32. Yang, J.; Huang, X. The 30 m annual land cover dataset and its dynamics in China from 1990 to 2019. *Earth Syst. Sci. Data* **2021**, *13*, 3907–3925. [CrossRef]
33. Pan, H.H.; Du, Z.Q.; Wu, Z.T.; Zhang, H.; Ma, K.M. Assessing the coupling coordination dynamics between land use intensity and ecosystem services in Shanxi's coalfields, China. *Ecol. Indic.* **2024**, *158*, 111321. [CrossRef]
34. Han, Z.L.; Meng, Q.Q.; Yan, X.L.; Zhao, W.Z. Spatial and temporal relationships between land use intensity and the value of ecosystem services in northern Liaodong Bay over the past 30 years. *Acta Ecol. Sin.* **2020**, *40*, 2555–2566. [CrossRef]
35. Hurst, H. Long term storage capacity of reservoirs. *Trans. Am. Soc. Civil. Eng.* **1951**, *6*, 770–799. [CrossRef]
36. Mandelbrot, B.; Wallis, J.R. Robustness of the rescaled range R/S in the measurement of noncyclic long-run statistical dependence. *Water Resour. Res.* **1969**, *5*, 967–988. [CrossRef]
37. Rivas-Tabares, D.A.; Saa-Requejo, A.; Martín-Sotoca, J.J.; Tarquis, A.M. Multiscaling NDVI series analysis of rainfed cereal in central Spain. *Remote Sens.* **2021**, *13*, 568. [CrossRef]
38. Chen, P.; Pan, H.Z.; Xu, Y.H.; He, W.X.; Yao, H.M. Spatial-Temporal evolution characteristics and driving force analysis of NDVI in Hubei Province, China, from 2000 to 2022. *Forests* **2024**, *15*, 719. [CrossRef]
39. Jiang, W.G.; Yuan, L.H.; Wang, W.J.; Cao, R.; Zhang, Y.F.; Shen, W.M. Spatio-temporal analysis of vegetation variation in the yellow river basin. *Ecol. Indic.* **2015**, *51*, 117–126. [CrossRef]
40. Tong, X.W.; Wang, K.L.; Brandt, M.; Yue, Y.M.; Liao, C.J.; Fensholt, R. Assessing future vegetation trends and restoration prospects in the karst regions of southwest China. *Remote Sens.* **2016**, *8*, 357. [CrossRef]
41. Yu, Y.Y.; Song, F.Y.; Zhang, S.J. Quantitative analysis of temporal and spatial changes of NDVI and Its driving factors in Henan province from 2000 to 2020. *Ecol. Environ. Sci.* **2022**, *31*, 1939–1950.

42. Chen, S.P.; Wang, W.Y.; Xu, W.T.; Wang, Y.; Wan, H.W.; Chen, D.M.; Tang, Z.Y.; Tang, X.L.; Zhou, G.Y.; Xie, Z.Q.; et al. Plant diversity enhances productivity and soil carbon storage. *Proc. Natl. Acad. Sci. USA* **2018**, *115*, 4027–4032. [CrossRef] [PubMed]
43. Yang, J.; Yan, D.M.; Yu, Z.L.; Wu, Z.N.; Wang, H.L.; Liu, W.M.; Liu, S.M.; Yang, Z. NDVI variations of different terrestrial ecosystems and their response to major driving factors on two side regions of the Hu-Line. *Ecol. Indic.* **2024**, *159*, 111667. [CrossRef]
44. Tuoku, L.; Wu, Z.; Men, B. Impacts of climate factors and human activities on NDVI change in China. *Ecol. Inform.* **2024**, *81*, 102555. [CrossRef]
45. Liu, Y.; Liu, H.H.; Chen, Y.; Gang, C.C.; Shen, Y.F. Quantifying the contributions of climate change and human activities to vegetation dynamic in China based on multiple indices. *Sci. Total Environ.* **2022**, *838*, 156553. [CrossRef] [PubMed]
46. Dai, Q.; Cui, C.F.; Wang, S. Spatiotemporal variation and sustainability of NDVI in the Yellow River basin. *Irrig. Drain.* **2022**, *71*, 1304–1318. [CrossRef]
47. Zheng, H.Y.; Miao, C.Y.; Li, X.Y.; Kong, D.X.; Gou, J.J.; Wu, J.W.; Zhang, S.P. Effects of vegetation changes and multiple environmental factors on evapotranspiration across China over the past 34 years. *Earth's Future* **2022**, *10*, e2021EF002564. [CrossRef]
48. Li, Y.Z.; Liu, C.M.; Liu, X.M.; Liang, K.; Bai, P.; Feng, Y.X. Impact of the Grain gor Green Project on the Land use/cover change in the Middle Yellow River. *J. Nat. Resour.* **2016**, *31*, 2005–2020. [CrossRef]
49. Liu, G.B.; Shangguan, Z.P.; Yao, W.Y.; Yang, Q.K.; Zhao, M.J.; Dang, X.H.; Guo, M.H.; Wang, G.L.; Wang, B. Ecological Effects of Soil Conservation in Loess Plateau. *Bull. Chin. Acad. Sci.* **2017**, *32*, 11–19. [CrossRef]
50. Wang, Y.F.; Chen, Y.P.; Wang, H.J.; Lv, Y.H.; Hao, Y.B.; Cui, X.Y.; Wang, Y.Z.; Hu, R.H.; Xue, K.; Fu, B.J. Ecosystem change and its ecohydrological effect in the Yellow River Basin. *Bull. Natl. Nat. Sci. Found. China* **2021**, *35*, 520–528. [CrossRef]
51. Song, W.Q.; Feng, Y.H.; Wang, Z.H. Ecological restoration programs dominate vegetation greening in China. *Sci. Total Environ.* **2022**, *848*, 157729. [CrossRef] [PubMed]
52. Dou, Y.J.; Wang, R.H.; Fu, H.P.; Zhang, Y.; Liu, R.J. Spatiotemporal variation and driving forces of NDVI in Shanxi Province. *Shanxi Univ. (Nat. Sci. Ed.)* **2023**, *46*, 244–255. [CrossRef]
53. Piedallu, C.; Chéret, V.; Denux, J.P.; Perez, V.; Azcona, J.S.; Seynave, I.; Gégout, J.C. Soil and climate differently impact NDVI patterns according to the season and the stand type. *Sci. Total Environ.* **2018**, *651*, 2874–2885. [CrossRef] [PubMed]
54. Zhang, H.X.; Chang, J.X.; Zhang, L.P.; Wang, Y.M.; Li, Y.Y.; Wang, X.Y. NDVI dynamic changes and their relationship with meteorological factors and soil moisture. *Environ. Earth Sci.* **2018**, *77*, 1–11. [CrossRef]
55. Suzuki, R.; Nomaki, T.; Yasunari, T. Spatial distribution and its seasonality of satellite-derived vegetation index (NDVI) and climate in Siberia. *Int. J. Climatol.* **2001**, *21*, 1321–1335. [CrossRef]
56. Gurgel, H.C.; Ferreira, N.J. Annual and interannual variability of NDVI in Brazil and its connections with climate. *Int. J. Remote Sens.* **2003**, *24*, 3595–3609. [CrossRef]
57. Eastman, J.R.; Sangermano, F.; Machado, E.A.; Rogan, J.; Anyamba, A. Global Trends in Seasonality of Normalized Difference Vegetation Index (NDVI), 1982–2011. *Remote Sens.* **2013**, *5*, 4799–4818. [CrossRef]
58. Olmos-Trujillo, E.; González-Trinidad, J.; Júnez-Ferreira, H.; Pacheco-Guerrero, A.; Bautista-Capetillo, C.; Avila-Sandoval, C.; Galván-Tejada, E. Spatio-Temporal Response of Vegetation Indices to Rainfall and Temperature in A Semiarid Region. *Sustainability* **2020**, *12*, 1939. [CrossRef]
59. Zhao, W.L.; Wang, H.Y.; Zhang, H.F.; Zhang, L. Precipitation and anthropogenic activities regulate the changes of NDVI in Zhegucuo Valley on the southern Tibetan Plateau. *J. Mt. Sci.* **2024**, *21*, 607–618. [CrossRef]
60. Gao, J.B.; Jiao, K.W.; Wu, S.H. Investigating the spatially heterogeneous relationships between climate factors and NDVI in China during 1982 to 2013. *Geogr. Sci.* **2019**, *29*, 1597–1609. [CrossRef]
61. Yuan, X.L.; Li, L.H.; Chen, X.; Shi, H. Effects of precipitation intensity and temperature on NDVI-Based grass change over northern China during the period from 1982 to 2011. *Remote Sens.* **2015**, *7*, 10164–10183. [CrossRef]
62. Flanagan, B.L.; Johnson, G.B. Interacting effects of temperature, soil moisture and plant biomass production on ecosystem respiration in a northern temperate grassland. *Agric. For. Meteorol.* **2005**, *130*, 237–253. [CrossRef]
63. Zhao, M.S.; Fu, C.B.; Yan, X.D.; Wen, G. Study on the relationship between different ecosystems and climate in china using NOAA/AVHRR data. *Acta Geogr. Sin.* **2001**, *56*, 287–296. [CrossRef]
64. Meng, Z.Q.; Liu, M.; Gao, C.C.; Zhang, Y.; She, Q.N.; Long, L.B.; Tu, Y.; Yang, Y.X. Greening and browning of the coastal areas in mainland China: Spatial heterogeneity, seasonal variation and its influential factors. *Ecol. Indic.* **2020**, *110*, 105888. [CrossRef]
65. Novick, A.K.; Ficklin, L.D.; Stoy, C.P.; Williams, A.C.; Bohrer, G.; Oishi, C.A.; Papuga, A.S.; Blanken, D.P.; Noormets, A.; Sulman, N.B.; et al. The increasing importance of atmospheric demand for ecosystem water and carbon fluxes. *Nat. Clim. Chang.* **2016**, *6*, 1023–1027. [CrossRef]
66. Williams, P.A.; Allen, D.C.; Macalady, K.A.; Griffin, D.; Woodhouse, A.C.; Meko, M.D.; Swetnam, W.T.; Rauscher, A.S.; Seager, R.; Grissino-Mayer, D.H.; et al. Temperature as a potent driver of regional forest drought stress and tree mortality. *Nat. Clim. Change* **2013**, *3*, 292–297. [CrossRef]
67. Yuan, W.P.; Zheng, Y.; Piao, S.L.; Ciais, P.; Lombaidozzi, D.; Wang, Y.P.; Ryu, Y.; Chen, G.X.; Dong, W.J.; Hu, Z.M.; et al. Increased atmospheric vapor pressure deficit reduces global vegetation growth. *Sci. Adv.* **2019**, *5*, eaax1396. [CrossRef]
68. Feng, X.H.; Li, Y.; Yu, E.; Yang, J.Y.; Wang, S.Y.; Ma, J.Y. Spatiotemporal pattern and coordinating development characteristics of carbon emission performance and land use intensity in the Yangtze River Delta Urban Agglomeration. *Trans. Chin. Soc. Agric. Eng. (Trans. CSAE)* **2023**, *39*, 208–218. [CrossRef]

69. Jin, K.; Wang, F.; Han, J.Q.; Shi, S.Y.; Ding, W.B. Contribution of climatic change and human activities to vegetation NDVI change over China during 1982–2015. *Acta Geogr. Sin.* **2020**, *75*, 961–974.
70. Fan, X.Y.; Gao, P.; Tian, B.Q.; Wu, C.X.; Mu, X.M. Spatio-Temporal patterns of NDVI and its influencing factors based on the ESTARFM in the Loess Plateau of China. *Remote Sens.* **2023**, *15*, 2072–4292. [CrossRef]
71. Zhu, Z.C.; Piao, S.L.; Myneni, R.B.; Huang, M.T.; Zeng, Z.Z.; Canadell, J.G.; Ciais, P.; Sitch, S.; Friedlingstein, P.; Arneth, A.; et al. Greening of the Earth and its drivers. *Nat. Clim. Chang.* **2016**, *6*, 791–795. [CrossRef]
72. Odasz-Albrigtsen, M.A.; Tømmervik, H.; Murphy, P. Decreased photosynthetic efficiency in plant species exposed to multiple airborne pollutants along the Russian-Norwegian border. *Can. J. Bot.* **2000**, *78*, 1021–1033.
73. Gupta, K.; Ghale, B.; Bhardwaj, A.; Varshney, A.; Khatriker, S.; Kumar, V.; Gupta, P.A.; Kumar, P. Urban Canopy Parameters' Computation and Evaluation in an Indian Context Using Multi-Platform Remote Sensing Data. *Urban. Sci.* **2024**, *8*, 191. [CrossRef]
74. Curdes, G. Urban morphology and climate change. Which morphology can survive. In Proceedings of the Seventeenth International Seminar on Urban Form, Hamburg, Germany, 20–23 August 2010.